PNAS RESEARCH ARTICLE | MICROBIOLOGY

Quantifying phage infectivity from characteristics of bacterial population dynamics

Michael Blazanin[a,b,c,1], Eli Vasen[a], Cèlia Vilaró Jolis[d], William An[a], and Paul E. Turner[a,b,c,e,1]

Contributed by Paul E. Turner; received May 25, 2025; accepted August 6, 2025; reviewed by Claudia Igler and Ing-Nang Wang

A frequent goal of phage biology is to quantify how well a phage kills a population of host bacteria. Unfortunately, traditional methods to quantify phage success can be time-consuming, limiting the throughput of experiments. Here, we use theory to show how the effects of phages on their hosts can be quantified using bacterial population dynamics measured in a high-throughput microplate reader (automated spectrophotometer). We use mathematical models to simulate bacterial population dynamics where specific phage and bacterial traits are known a priori. We then test common metrics of those dynamics (e.g., growth rate, time and height of peak bacterial density, death rate, extinction time, area under the curve) to determine which best predict: 1) infectivity over the short-term, and 2) phage suppression over the long term. We find that many metrics predict infectivity and are strongly correlated with one another. We also find that metrics can predict phage growth rate, providing an effective way to quantify the combined effects of multiple phage traits. Finally, we show that peak density, time of peak density, and extinction time are the best metrics when comparing across different bacterial hosts or over longer timescales where plasticity or evolution may play a role. In all, we establish a foundation for using bacterial population dynamics to quantify the effects of phages on their bacterial hosts, supporting the design of in vitro empirical experiments using microplate readers.

methods development | theory | simulations

Significance

Bacteriophages are viruses that infect bacteria, with relevance from basic science to medical application. Frequently, we seek to quantify how these viruses negatively impact bacterial growth. Typical methods are labor-intense, limiting the number of experiments that can be done. Here, we show how easily collectable data (called "bacterial population dynamics" or "growth curves") can be used to quantify virus killing of bacteria across a wide range of conditions. In all, our work suggests that these dynamics provide an effective and high-throughput method to quantify phage effects on their hosts.

In the study of lytic bacteriophages (phages), a common experimental goal is to quantify how well a phage can kill a given bacterial strain. This question is asked both on short timescales as well as over longer timescales. On short timescales, we want to quantify "infectivity", which we define as how well a specific phage strain infects and kills a specific bacterial strain. At this timescale, we expect that phage and bacterial phenotypes are mainly constant, and that infectivity reflects both: 1) the phage's ability to infect host cells, as well as 2) the bacterium's ability to resist phage attack (1, 2). On longer timescales, plasticity and evolution can come into play, allowing phage and bacterial phenotypes to change. In this case, we want to quantify the magnitude and duration of phage-driven suppression of the bacterial population, even as bacteria become resistant to phages. Unfortunately, experimentally quantifying phage success over the short or long term can require time-consuming methods, limiting the throughput of experiments (3–8).

Here, we aim to show how the success of obligately lytic phages over both the short and long term can be quantified in high-throughput from bacterial population dynamics estimated in a microplate reader ("growth curves," e.g., as measured with optical density). Many groups have measured proxies of bacterial density over time in the presence and absence of phages in order to qualitatively infer phage activity (9–36). In addition, some studies have proposed ways to use population dynamics to quantify infectivity (37–50), attempting to extract a metric (or metrics) from the time series of bacterial densities that reflects infectivity. However, which of these proposed approaches best reflect infectivity, and whether they can be extended to quantify phage success over longer timescales with plasticity or evolution, has not been systematically tested.

To address this gap, we used mathematical models to simulate bacterial population dynamics in the presence and absence of infecting phages (*SI Appendix*, Fig. S1). Such models have been widely used to study phage-bacteria interactions (51–53), but only rarely applied to understand how population dynamics could be used to quantify phage success (45, 47). By modeling, we can simulate and compare bacterial population dynamics where bacterial and phage traits are precisely controlled and known a priori. Using our models, we complement the existing body of largely empirical papers (37–50) to show that many metrics predict infectivity, are strongly correlated with one another, and can be used to infer phage growth rate, providing an effective way to quantify the combined effects of multiple phage traits. Additionally, we find that peak density, time of peak

Author affiliations: [a]Department of Ecology and Evolutionary Biology, Yale University, New Haven, CT 06520; [b]Center for Phage Biology & Therapy, Yale University, New Haven, CT 06520; [c]Quantitative Biology Institute, Yale University, New Haven, CT 06520; [d]Department of Biochemistry, Universitat de Barcelona, Barcelona 08014, Spain; and [e]Program in Microbiology, Yale School of Medicine, New Haven, CT 06536

Preprint server: https://doi.org/10.1101/2023.06.29.546975.

Author contributions: M.B. and P.E.T. designed research; M.B., E.V., C.V.J., and W.A. performed research; M.B. analyzed data; and M.B. and P.E.T. wrote the paper.

Reviewers: C.I., The University of Manchester Faculty of Biology Medicine and Health; and I.-N.W., University at Albany.

The authors declare no competing interest.

[1]To whom correspondence may be addressed. Email: mikeblazanin@gmail.com or paul.turner@yale.edu.

This article contains supporting information online at https://www.pnas.org/lookup/suppl/doi:10.1073/pnas.2513377122/-/DCSupplemental.

Published September 8, 2025.

Table 1. Model parameter terms and their definitions

Parameter	Definition	Default Value [Range of values]
u_S	Maximum per-capita growth rate of susceptible cells	0.0179 [0.00798 to 0.04] /min (doubling time of ~39 [87 to 17] min)
k	Stationary phase density of cells	10^9 [10^8 to 10^{10}] CFU/mL
a	Maximum adsorption rate of susceptible cells by free phage particles	10^{-10} [10^{-12} to 10^{-8}] infections/cell/phage/mL/min
b	Burst size: number of phages produced by each infected cell	50 [5 to 500] phages/cell
τ	Lysis time, the lag between infection of a susceptible cell and lysis to release new phages	31.6 [10 to 100] min
z	Scaling parameter for rate of superinfection of infected cells by free phages relative to rate of infection of susceptible cells	1 [0 to 1]
d	Fraction of nutrients replenished by each cell death	0 [0 to 1]
h	Transition rate of susceptible cells to resistant cells, relative to growth rate	0 [0, 10^{-8} to 10^{-1}]
u_R	Maximum per-capita growth rate of resistant cells	0 [0 to 0.0179] /min
f_a	Degree of adsorption rate plasticity	0 [0 to 3]
S_0	Initial density of susceptible cells	10^6 [10^6 to 10^8] CFU/mL
I_0	Initial density of infected cells	0 CFU/mL
P_0	Initial density of phages	10^4 [10^4 to 10^6] PFU/mL
N_0	Initial density of nutrients	$k - S_0 - I_0$CFU/mL

Unless otherwise noted, all simulations used the default value listed. For the noted exceptions, simulations typically used the range of values in brackets, which approximately span the experimentally observed ranges of phenotypes (*SI Appendix*, Table S1).

density, and extinction time are the best metrics when bacterial hosts vary in their growth or over longer timescales where plasticity or evolution may play a role.

Materials and Methods

Overview. We used the common approach of modeling populations of susceptible bacteria, infected bacteria, free phage particles, and nutrients with a system of differential equations (*SI Appendix*, Fig. S1). These equations track the densities of each of the four populations over time, linking the effects of each population on the others through mathematical terms for processes like growth, infection, and lysis. Such terms also include parameters like growth rate, stationary phase density, adsorption rate (assuming all adsorption events lead to infection), burst size (number of phages produced by each infected cell), and lysis time (the time delay between infection of a susceptible cell and lysis to release new phage particles). By simulating population dynamics with different parameter values, we can then observe how changes in each parameter value alter the observed bacterial population dynamics. Finally, we can apply the various approaches to analyze growth curves from the literature to our simulated data, enabling us to directly test the efficacy of each approach.

Main Model of Bacterial Population Dynamics. We built a delay differential equation model of bacterial and phage growth (54) (Eqs. **1** – **4**) with populations of susceptible bacteria (S), infected bacteria (I), free phages (P), and nutrients (N). The nutrient population is defined in units of cells, so that one unit of nutrients yields one cell. In this model, nutrients can return into the environment from cell lysis at a rate controlled by the d parameter. Note that when $d = 1$ (i.e., the lysis of one cell returns one cell's worth of nutrients back into the environment), this model simplifies to logistic growth. For convenience, we let k be the stationary phase density of cells, and let $N_0 = k - S_0 - I_0$. Subscripts denote time (i.e., S_t is the population of susceptible cells at time t). Descriptions of all parameters are provided in Table 1.

$$\frac{dS}{dt} = uS_t\frac{N_t}{k} - aS_tP_t, \quad [1]$$

$$\frac{dI}{dt} = aS_tP_t - aS_{t-\tau}P_{t-\tau}. \quad [2]$$

$$\frac{dP}{dt} = -aS_tP_t + baS_{t-\tau}P_{t-\tau} - azI_tP_t, \quad [3]$$

$$\frac{dN}{dt} = -uS_t\frac{N_t}{k} + daS_{t-\tau}P_{t-\tau}. \quad [4]$$

This model produces growth curves under the assumption that bacteria remain fully susceptible to phage infection at all times (Figs. 1–7). However, susceptibility to phage infection is known to decline as bacterial growth and metabolism slow as the population enters the stationary phase (51, 55–59). We identified simulated growth curves where this assumption is likely violated when $S + I \geq 0.9 * k$ at any point in time. In some plots in the main text, these simulations are excluded (as noted in the figure legends), but plots with all simulations are included in the supplement.

Models of Bacterial Population Dynamics with Plasticity or Evolution. To explicitly model changes in bacterial susceptibility over time via plasticity or evolution (Fig. 8), we used previously published approaches (51) to model three scenarios. In the first scenario, as nutrient density and bacterial growth rate decline, phage growth slows via decreases in the adsorption rate [Eqs. **5** – **9**, (60)] or burst size (*SI Appendix*, Appendix 9), or increases in lysis time (*SI Appendix*, Appendix 9). Here, a_t declines linearly with decreasing nutrient availability. The slope of that decline, and the total decrease when nutrients have been completely depleted, is controlled by the f parameter.

$$\frac{dS}{dt} = uS_t\frac{N_t}{k} - a_tS_tP_t, \quad [5]$$

$$\frac{dI}{dt} = a_tS_tP_t - a_{t-\tau}S_{t-\tau}P_{t-\tau}, \quad [6]$$

$$\frac{dP}{dt} = -a_tS_tP_t + ba_{t-\tau}S_{t-\tau}P_{t-\tau} - a_tzI_tP_t, \quad [7]$$

$$\frac{dN}{dt} = -uS_t\frac{N_t}{k} + da_{t-\tau}S_{t-\tau}P_{t-\tau}, \quad [8]$$

where

$$a_t = a * \max\left(0, 1 - f_a + f_a\frac{N_t}{k}\right), \quad [9]$$

In the second and third scenarios, bacterial cells transition into a resistant state (Eqs. **10** – **12**), either because of plastic changes conferring a nongrowing resistant state ($u_R = 0$), or evolutionary mutations conferring cost-free resistance

($u_R > 0$) [*SI Appendix*, Appendix 9, (61)]. Descriptions of all parameters are provided in Table 1.

$$\frac{dS}{dt} = u_S S_t \frac{N_t}{k} - aS_t P_t - hu_S S_t, \quad [10]$$

$$\frac{dR}{dt} = u_R R_t \frac{N_t}{k} + hu_S S_t, \quad [11]$$

$$\frac{dN}{dt} = -u_S S_t \frac{N_t}{k} - u_R R_t \frac{N_t}{k}. \quad [12]$$

Simulation Implementation and Analysis. Simulated population dynamics data were generated using deSolve (62), using default values for all parameters (Table 1) for 48 h of simulated time unless otherwise noted. Data were analyzed using gcplyr (63): Maximum growth rate was calculated using a sliding window 5 data points wide on non-log-transformed data, 10^4 CFU/mL was used as the arbitrary threshold for extinction time, and 10^6 CFU/mL was used as the arbitrary threshold for emergence time. Principal component analyses were carried out using each timepoint as a variable, using either the raw density values or (for "normalized PCA") the difference in density values from a control with no phages added. Relative area under the curve (AUC) in Fig. 7 was calculated as AUC divided by the AUC of a control curve with no phages added. The coefficient of variation in Fig. 7 is the SD divided by the mean. All code used to generate, analyze, and visualize data in R v4.4.3 is available at https://github.com/mikeblazanin/growth-curves.

Results

First, we tested how changes in phage traits (burst size, lysis time, and adsorption rate) alter the shape of the curves of bacterial population dynamics. Regardless of the phage trait that varies, we observe that all bacterial populations still display a characteristic exponential phase, before the population density peaks and then rapidly declines due to phage killing (Fig. 1). Notably, phage traits do not substantially alter the bacterial population's density or growth rate during the initial exponential phase, even though our simulations assume cells cease growth immediately upon infection. We and others have observed such a pattern empirically [*SI Appendix*, Appendix 8, (19, 36, 40, 41, 43–47, 49, 64, 65)], which arises because infection remains rare during the exponential phase.

Next, we tested how changes in phage traits affect the various metrics that have been proposed (4, 37–46, 48, 50) to quantify phage infectivity from bacterial population dynamics. As expected from the patterns in bacterial population dynamics in Fig. 1, metrics like the bacterial growth rate (38, 41), time to reach a threshold density (39, 42), and rate of population decline (41) do not correlate with phage adsorption rate (Fig. 2 *A*, *B*, and *E*), burst size (*SI Appendix*, Fig. S2), or lysis time (*SI Appendix*, Fig. S3). In contrast, metrics like the height and timing of the peak bacterial density (45, 47), the timing of bacterial population extinction (45), the area under the curve (38, 40, 43, 44, 46, 48), and multivariate principal component analyses (37, 48) correlate strongly with phage adsorption rate (Fig. 2 *C*, *D*, and *F*–*H*), burst size (*SI Appendix*, Fig. S2), and lysis time (*SI Appendix*, Fig. S3).

Next, we tested whether metrics calculated from bacterial population dynamics are correlated with each other, since it remains unclear how these different metrics compare to one another and whether they provide redundant versus complementary information about phage infectivity. We find that different metrics are extremely tightly correlated with one another, suggesting that they provide redundant information (Fig. 3 and *SI Appendix*, Fig. S4).

Thus far, we have shown that metrics calculated from bacterial population dynamics correlate strongly with each other and with the phage traits of burst size, lysis time, and adsorption rate.

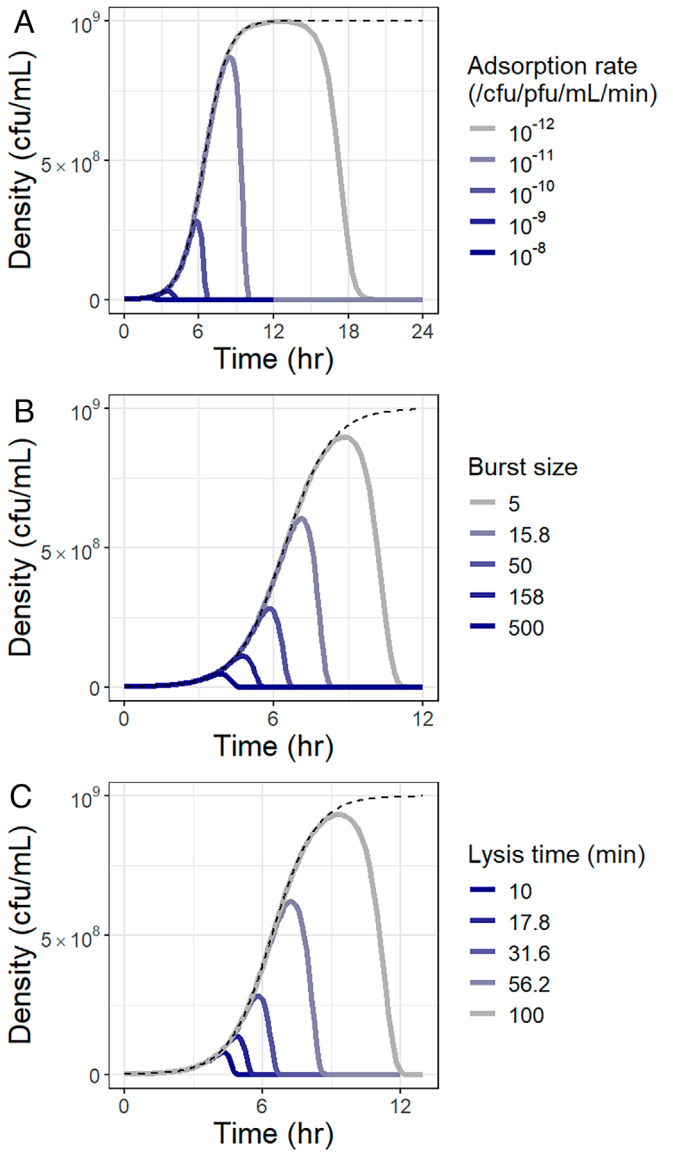

Fig. 1. Phage infectivity alters peak and death phases of bacterial population dynamics, but not exponential phase. Bacterial population dynamics were simulated with phages with varying adsorption rates (*A*), burst sizes (*B*), or lysis times (*C*), plotting the total bacterial density over time. The dashed line denotes bacterial growth in the absence of phages.

However, many experiments do not go to the level of quantifying specific phage traits, instead quantifying overall phage growth. Here, we find that metrics calculated from bacterial population dynamics are also strongly correlated with average phage growth rate (Fig. 4 and *SI Appendix*, Appendix 4). These findings are consistent with past in vitro and in silico work (45, 47) and suggest that lytic phage growth rate can be inferred simply by quantifying the observable effects the phage has on the population density of its bacterial host.

We next quantified how the phage traits of burst size, lysis time, and adsorption rate interact with each other in altering bacterial population dynamics, as well as quantifying how strongly each trait affects the metrics calculated from bacterial population dynamics. All three traits contribute substantially to shaping bacterial population dynamics (Fig. 5 and *SI Appendix*, Figs. S6–S10), frequently interacting with diminishing returns (*SI Appendix*, Fig. S11). Of the three traits, lysis time typically has the strongest absolute effect (Fig. 5*D* and *SI Appendix*, Fig. S12); that is, a given

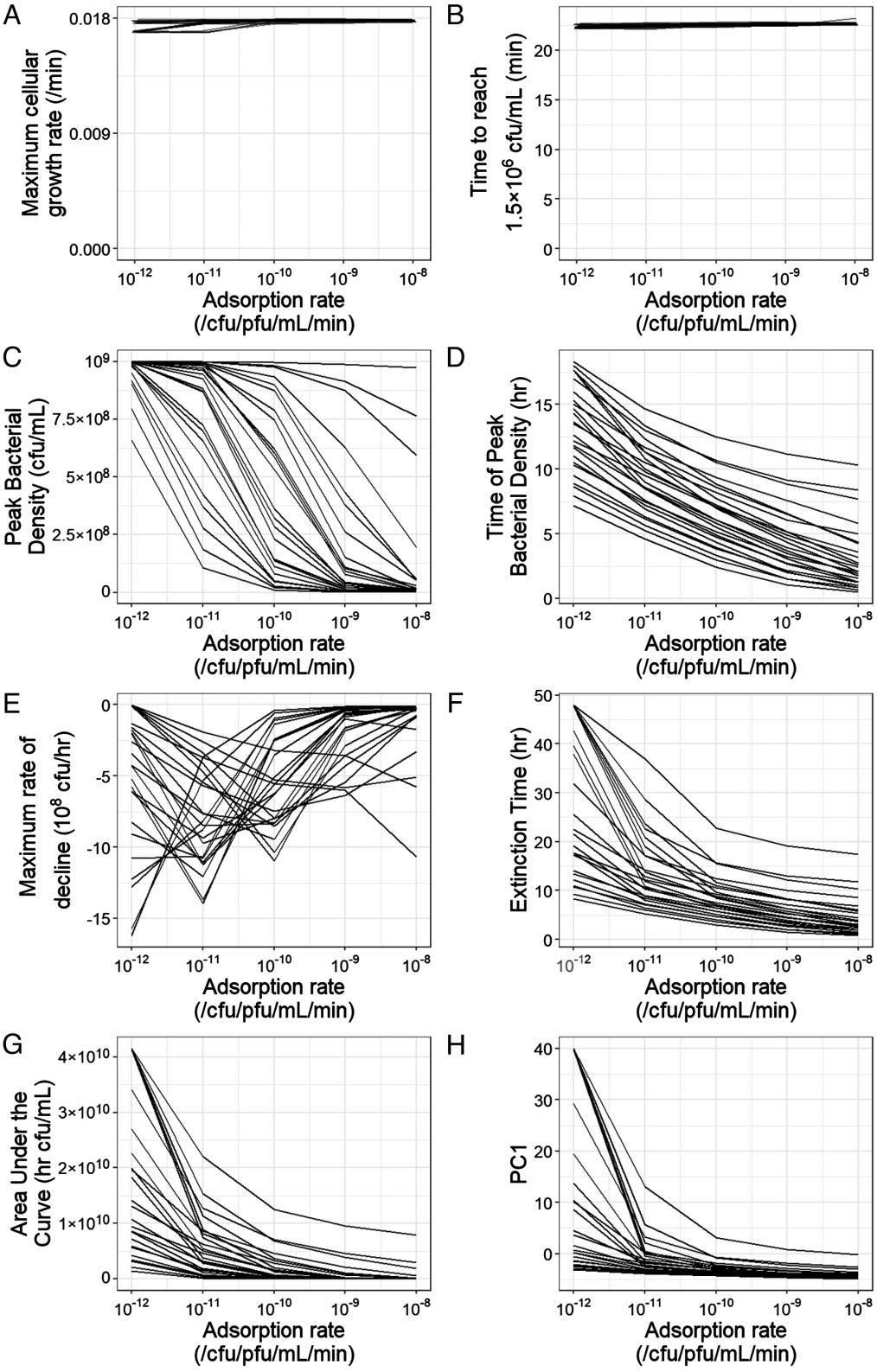

Fig. 2. Metrics of the exponential phase and rate of decline do not correlate with phage infectivity, while metrics of peak, overall growth, and timing of death phase do correlate with phage infectivity. (*A*–*H*) Bacterial population dynamics were simulated for 48 h with phages with all combinations of varying adsorption rates, lysis times (10, 17.8, 31.6, 56.2, 100 min), and burst sizes (5, 15.8, 50, 158, 500 PFU/infection). Each line plots the metrics calculated from bacterial population dynamics with phages having the same lysis time and burst size, across varying adsorption rates. (*A* and *B*) Small amounts of jitter in both the x and y direction were added to aid visualization of many overlapping lines. (*F*) Six populations did not reach the extinction threshold and are plotted as 48 h. (*H*) PC1 is the first principal component from a principal component analysis of the bacterial population dynamics.

fold-change in lysis time has a larger effect than the same fold-change in burst size or adsorption rate. However, the three traits are not equally variable: Adsorption rate has the widest range of natural variation, followed by burst size, then lysis time (*SI Appendix*, Table S1, 66–79). If we normalize to compare across the full range of natural variation, adsorption rate often has the

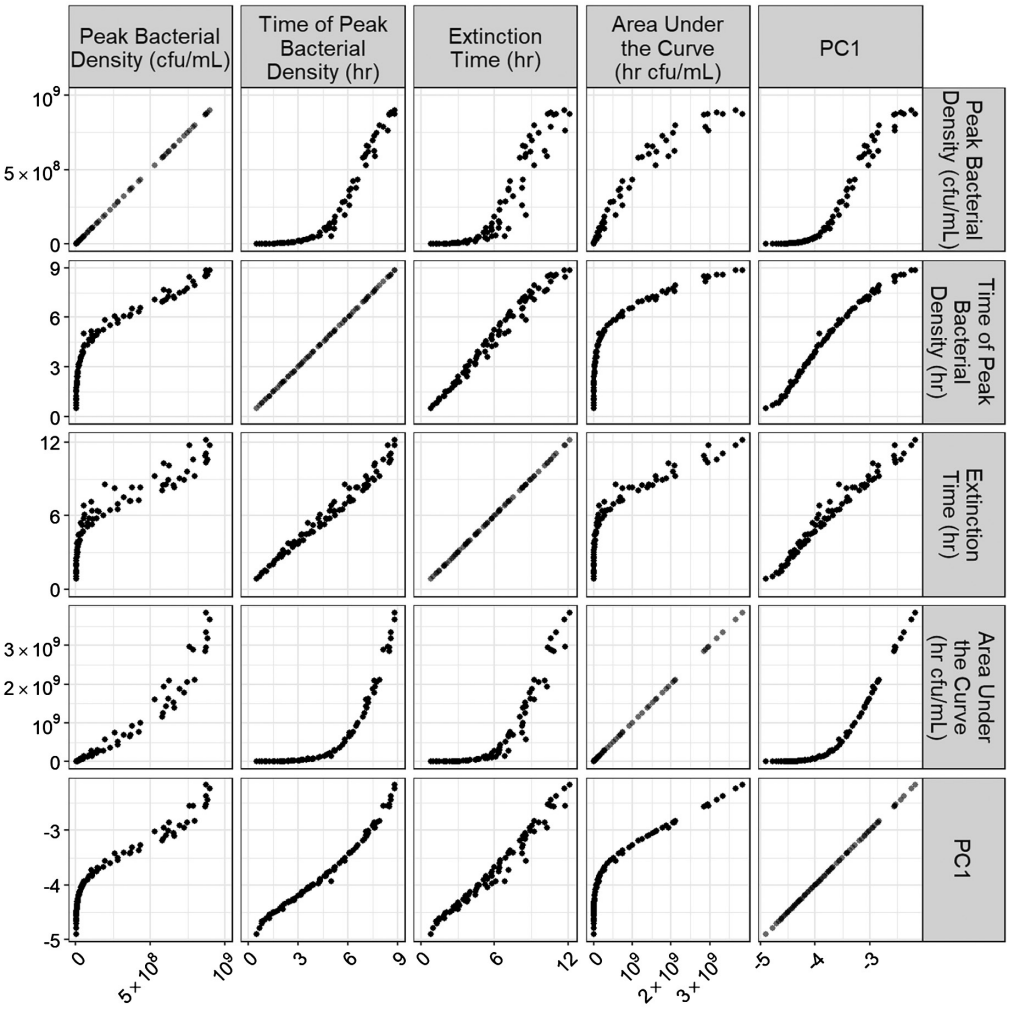

Fig. 3. Metrics of bacterial population dynamics are tightly correlated with each other. Bacterial population dynamics were simulated with phages with all combinations of varying adsorption rates (10^{-12}, 10^{-11}, 10^{-10}, 10^{-9}, 10^{-8} /CFU/PFU/mL/min), lysis times (10, 17.8, 31.6, 56.2, 100 min), and burst sizes (5, 15.8, 50, 158, 500 PFU/infection). Bacterial populations which approximately reached their stationary phase density are excluded from this plot (*SI Appendix*, Fig. S4). PC1 is the first principal component from a principal component analysis of the bacterial population dynamics.

largest effect (Fig. 5*E* and *SI Appendix*, Fig. S12). Regardless, these data show that metrics of bacterial population dynamics provide an effective way to quantify the combined effects of multiple phage traits without measuring individual phage traits.

Next, we tested how strongly the initial densities of bacteria and phages affect the metrics calculated from bacterial population dynamics. Initial densities can substantially alter bacterial population dynamics, with initial bacterial density typically having a stronger effect than initial phage density (Fig. 6 and *SI Appendix*, Appendix 6 and Figs. S13–S15). Fortunately, both initial bacterial density and initial phage density typically have weaker effects on bacterial population dynamics than phage infectivity, so although initial densities do need to be experimentally controlled, random noise in inoculation densities should not obscure differences in infectivity (*SI Appendix*, Appendix 6 and Figs. S16 and S17). Additionally, in contrast to the strong interactions between traits in determining population dynamic metrics (Fig. 5 and *SI Appendix*, Appendix 5), the effects of log initial phage and log bacterial density are approximately linear on many metrics (Fig. 6 and *SI Appendix*, Appendix 6). Thus, experimenters can manipulate initial bacterial and phage density to maximize the signal of phage infectivity between strains (*SI Appendix*, Fig. S14 *C* and *D*).

We now set out to test how metrics of population dynamics can be used to compare phage infectivity across different bacterial hosts, for instance, when bacterial strains vary in their resistance to infection. Many population dynamic metrics used to infer infectivity can be strongly affected by variation in bacterial traits like growth rate or stationary phase density (Fig. 7 and *SI Appendix*, Appendix 7). Of the metrics, the time of peak bacterial density and extinction time tend to be the best metrics (i.e., are least affected by variation in bacterial traits). One proposed approach to explicitly account for variation in bacterial traits is to calculate the area under the curve (AUC) relative to the AUC of a control where bacteria are grown alone (40, 44, 46). When bacterial strains vary in their growth rate, relative AUC can be a somewhat better indicator than raw AUC of infectivity (Fig. 7*A*). However, counterintuitively, when bacterial strains vary in their stationary phase density, relative AUC is actually a much worse indicator of infectivity (Fig. 7*B*). This arises because phages typically cause bacterial populations to collapse before they begin to approach stationary phase, so AUC values vary more in the control than in the presence of phages. A second approach to explicitly account for variation in bacterial traits is to use multivariate ordination methods like PCA on the raw density values or the density values relative to those of a control where bacteria are grown alone (37, 48). When bacteria vary in growth rate, both PCA approaches work well as metrics of infectivity, with little overall improvement from PCA on relative densities (Fig. 7*A*). However, when bacterial strains

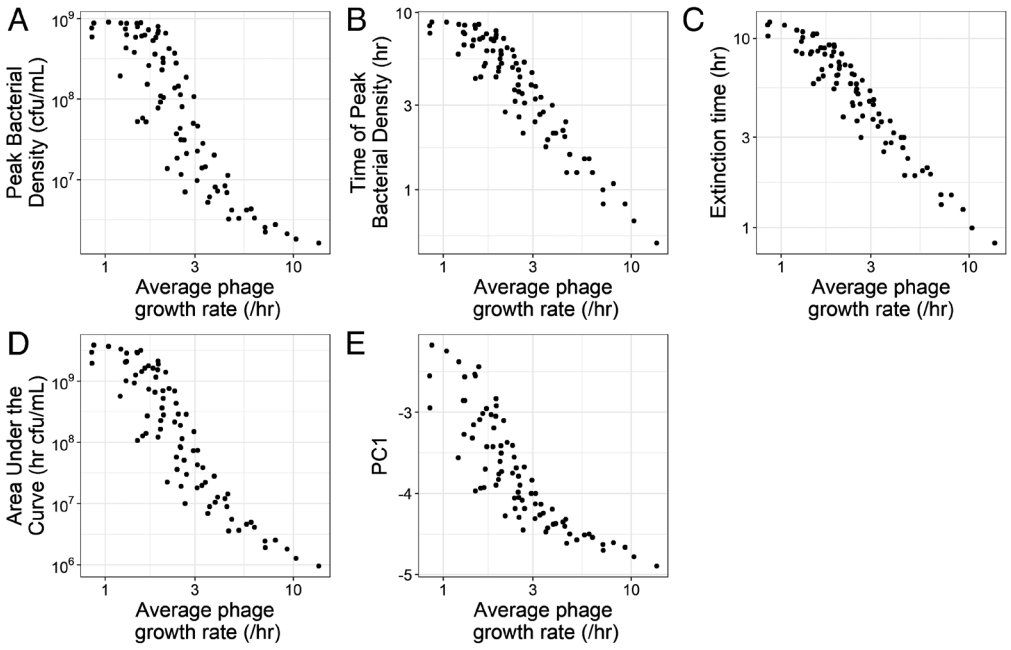

Fig. 4. Metrics of bacterial population dynamics are correlated with phage growth rate. (*A*–*H*) Bacterial population dynamics were simulated with phages with all combinations of varying adsorption rates (10^{-12}, 10^{-11}, 10^{-10}, 10^{-9}, 10^{-8} /CFU/PFU/mL/min), lysis times (10, 17.8, 31.6, 56.2, 100 min), and burst sizes (5, 15.8, 50, 158, 500 PFU/infection). Populations which approximately reached their stationary phase density are not plotted here (*SI Appendix*, Fig. S5). The average phage growth rate was calculated as $\frac{\log(P_{final}/P_0)}{t_{final}}$ using the extinction time as the final timepoint. (*E*) PC1 is the first principal component from a principal component analysis of the bacterial population dynamics.

vary in their stationary phase density, PCA on relative densities is a much worse metric of phage infectivity (Fig. 7*B*). This arises for much the same reason as AUC: When bacteria vary in stationary phase density, control densities vary more than densities in the presence of phages.

Finally, we sought to test how bacterial population dynamics can be used to quantify the effects of phages over longer timescales, when bacteria can become resistant through plastic or evolutionary changes. For instance, in vitro bacterial susceptibility is often observed to decline as bacterial growth slows (51, 55–59), and bacteria are also known to readily evolve resistance against phages. To assess these effects on bacterial population dynamics, we used previously published approaches (51) to simulate three scenarios (Fig. 8 and *SI Appendix*, Appendix 9):

1) Phage growth weakening as bacterial growth slows (20, 51, 57, 60, 80, 81). Here, we find that bacterial population dynamics are substantially altered if bacteria reach stationary phase (Fig. 8*A*). There, bacterial growth slows enough that phage growth falls to zero, preventing the collapse observed in previous simulations. This also makes it impossible to distinguish phage infectivity differences between any bacterial populations that are sufficiently resistant to reach stationary phase (Fig. 8*D*).
2) Bacterial cells transitioning into a phenotypically resistant state (61). Here, transitions into a phenotypically resistant state can produce patterns of partial population collapse (Fig. 8 *B* and *E*) that have been observed empirically [(9), *SI Appendix*, Fig. S21], although such patterns in optical density can also be explained by debris (*SI Appendix*, Fig. S27).
3) Bacteria evolving mutations that confer resistance to phage infection. Here, bacterial populations collapse to near-zero densities before rebounding because of the evolution of phage-resistant mutants (Fig. 8*C*).

Across all three scenarios, metrics like final density or re-emergence time reflect both infectivity and the degree/rate of plasticity or evolution (Fig. 8 *D*–*F*), while metrics like peak density, time of peak density, and extinction time remain good indicators of phage infectivity alone, independent of the effects of plasticity or evolution (*SI Appendix*, Fig. S29).

Discussion

Here, we set out to test how bacterial population dynamics can be used to quantify phage infectivity (and bacterial resistance), using mathematical models to simulate population dynamics with known trait values. We showed that many, but not all, metrics of bacterial population dynamics reflect phage infectivity (Fig. 2) and that metrics are strongly correlated with one another (Fig. 3). We then showed that these metrics can be used to infer phage growth rate (Fig. 4), providing an effective way to quantify the combined effects of multiple phage traits (Fig. 5). We also showed that metrics can be somewhat affected by initial inoculum densities (Fig. 6) and identified time of peak density and extinction time as the best metrics to compare across different bacterial hosts (Fig. 7). Finally, we showed that the effects of phages can sometimes be inferred over longer time-scales where bacterial plasticity or evolution can alter population dynamics (Fig. 8).

Observation of bacterial population dynamics complements existing methods for estimating phage infectivity. Existing methods often exhibit tradeoffs between throughput and precision (3, 4), with some approaches (e.g., efficiency of plaquing) providing quantitative but low-throughput measures of infectivity (5–7), while others (e.g., cross-streaks) provide qualitative but high-throughput measures of infectivity (8). In contrast, bacterial population dynamics can be easily scaled to collect many replicates in parallel and can produce quantitative measures of infectivity, albeit with a smaller range of detection (~2 orders of magnitude in infectivity, Fig. 2*C*). In addition, inferring phage infectivity

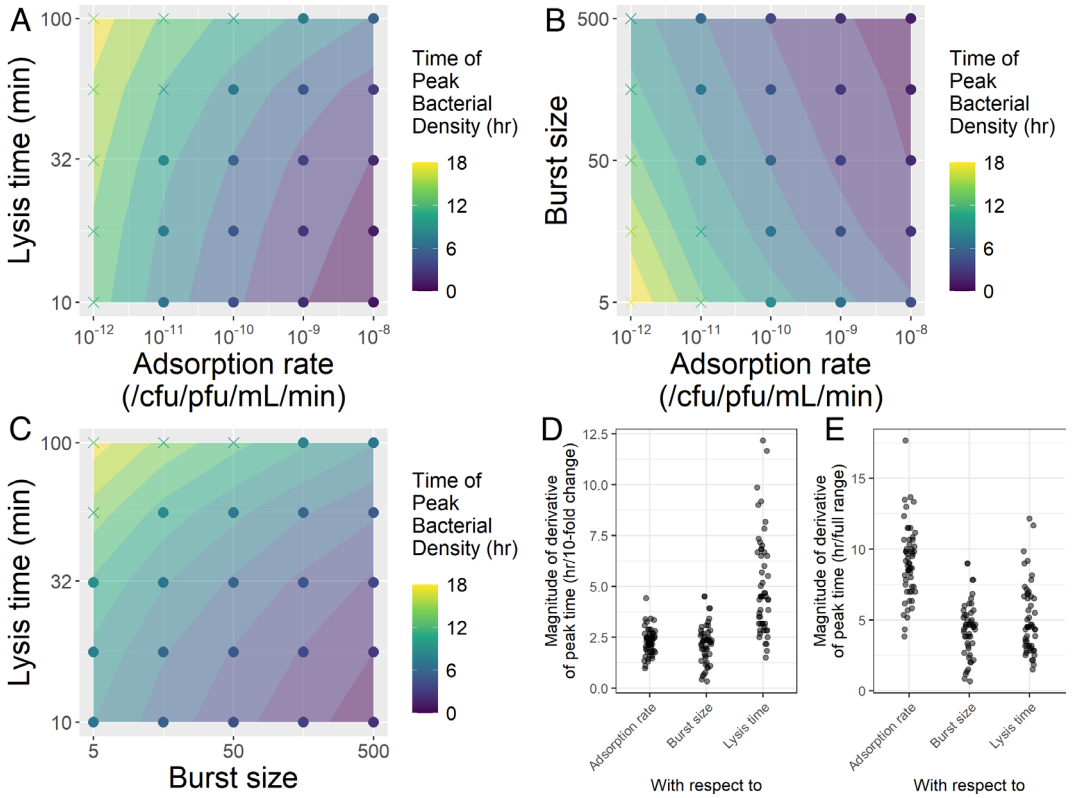

Fig. 5. Phage traits jointly determine time of peak bacterial density. Bacterial population dynamics were simulated with phages with all combinations of varying adsorption rates (10^{-12}, 10^{-11}, 10^{-10}, 10^{-9}, 10^{-8} /CFU/PFU/mL/min), lysis times (10, 17.8, 31.6, 56.2, 100 min), and burst sizes (5, 15.8, 50, 158, 500 PFU/infection). Plotted are subsets of the simulations where (*A*) burst size = 50, (*B*) lysis time = 31.6 min, or (*C*) adsorption rate = 10^{-10} /cfu/pfu/mL/min. Bacterial populations which approximately reached their stationary phase density are plotted as "x"s. (*D*) We calculated the magnitude (i.e., absolute value) of the rate of change of the time of peak bacterial density against a 10-fold change in each phage trait. (*E*) We calculated the magnitude (i.e., absolute value) of the rate of change of the time of peak bacterial density against each phage trait normalized to have a range of 1. Populations which approximately reached their stationary phase density are not plotted in *D* and *E* (*SI Appendix*, Fig. S12).

from bacterial population dynamics may better reflect phage-bacteria interactions in liquid environments than the existing agar surface-based methods for observing phage infectivity, although further work is needed.

Our work builds on prior papers that used bacterial population dynamics to infer phage activity (37–50). However, our findings contrast with some of their previously reported results. For example, several papers have suggested using normalized area under the curve (40, 44, 46) or PCA (37) to compare infectivity across bacterial hosts, but we find that these metrics are not particularly well suited to this task and in some cases are worse than the unnormalized metrics (Fig. 7). Additionally, two recent papers have suggested fitting mathematical models to bacterial population dynamics to extract phage trait values (47, 49). Although we did not directly explore fitting-based approaches, so they remain an avenue for future theoretical work, our findings that metrics strongly covary (Fig. 3) and that many combinations of trait values can produce similar curves (Fig. 5) would suggest that bacterial population dynamics are unlikely to be sufficient to quantify specific phage life history traits like adsorption rate, burst size, or lysis time. At the same time, our findings do align with some previously reported results. For instance, we found that the exponential phase of population dynamics provides little

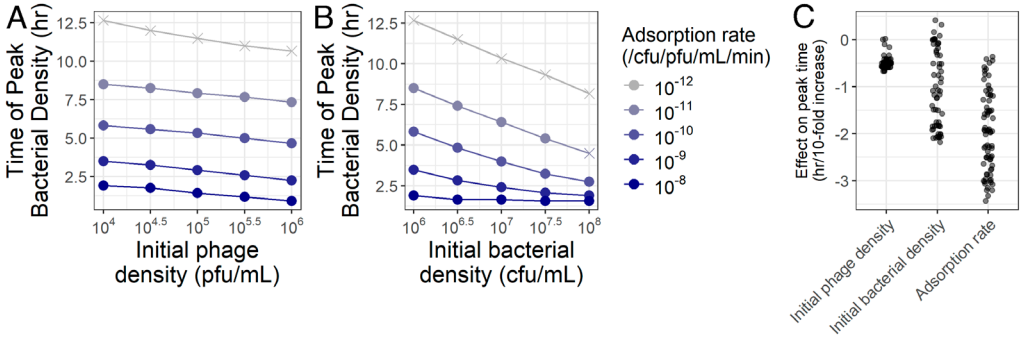

Fig. 6. Metrics of bacterial population dynamics can be sensitive to inoculation densities. Bacterial population dynamics were simulated with phages with all combinations of varying adsorption rates and initial phage (*A*) or bacterial (*B*) densities (while holding the other constant). Bacterial populations which approximately reached their stationary phase density are plotted as "x"s. (*A*) The initial density of bacteria was held constant at 10^6 CFU/mL. (*B*) The initial density of phages was held constant at 10^4 PFU/mL. (*C*) We calculated the magnitude of the rate of change of the time of peak bacterial density against a 10-fold change in adsorption rate, initial bacterial density, or initial phage density. Populations which approximately reached their stationary phase density are not plotted (*SI Appendix*, Fig. S15).

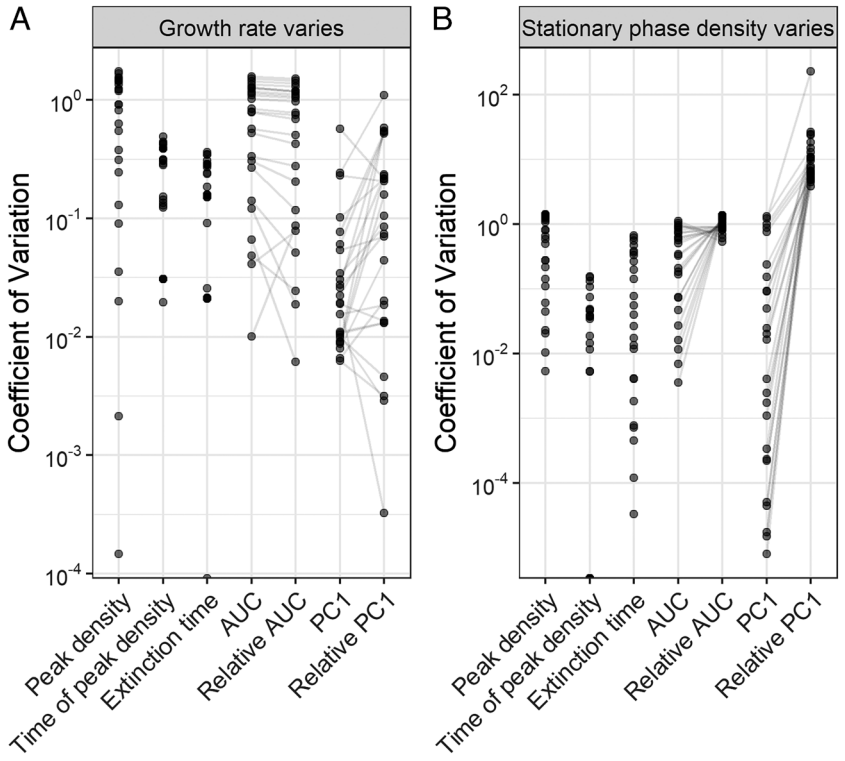

Fig. 7. When bacteria vary, the time of peak bacterial density and extinction time are the best metrics of phage infectivity. Bacterial population dynamics were simulated with phages with all combinations of varying adsorption rates (10^{-12}, 10^{-11}, 10^{-10}, 10^{-9}, 10^{-8} /CFU/PFU/mL/min) and bacteria with varying stationary phase densities (10^{8}, $10^{8.5}$, 10^{9}, $10^{9.5}$, 10^{10} CFU/mL) and growth rates (0.04, 0.027, 0.018, 0.012, 0.008 /min; doubling times of 17, 26, 39, 58, and 87 min). We then calculated the amount of variation in each metric among simulations with (*A*) the same adsorption rate and stationary phase density, or (*B*) the same adsorption rate and growth rate. Smaller coefficients of variation indicate that the measure is a better indicator of infectivity across bacteria that vary in *A*. growth rate, or *B*. stationary phase density. For AUC and Relative AUC, and PC1 and Relative PC1, lines connect sets of simulations with the same parameter values.

information about phage infectivity (Fig. 1), a pattern that has been observed in our own empirical data (*SI Appendix*, Appendix 8), previous phage-bacteria studies (19, 36, 40, 41, 43–47, 49), and in epidemiology (82, 83). Our simulations also reproduced previously reported near-linear relationships between phage growth rate and bacterial extinction time [Fig. 4*C*, (45)], peak bacterial density and initial phage density [*SI Appendix*, Fig. S14*B*, (47)], and time of peak bacterial density and initial bacterial density [Fig. 6*B*, (49)].

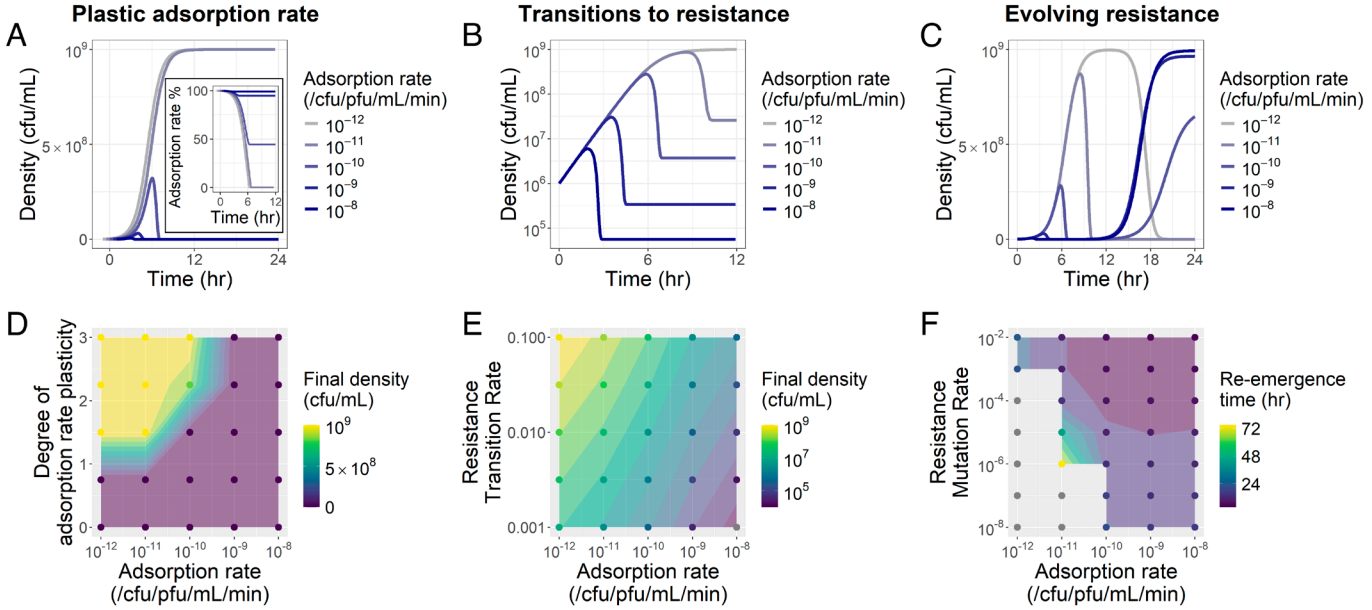

Fig. 8. Plasticity and evolution can alter the shape of bacterial population dynamics over longer timescales.(*A*–*F*) Bacterial population dynamics were simulated with phages with varying adsorption rates (10^{-12}, 10^{-11}, 10^{-10}, 10^{-9}, 10^{-8} /CFU/PFU/mL/min). (*A*) Phages were simulated with an adsorption rate that declines linearly with declining bacterial growth rate (f_a = 1.5). Bacterial populations that reach stationary phase fast enough that the phage adsorption rate reaches 0 (*Inset*) can persist without ever crashing. Population densities and adsorption rates have been slightly offset horizontally for visualization. (*B*) Bacteria were simulated with transitions into a nongrowing resistant state (h = 0.01). (*C*) Bacteria were simulated with cost-free mutations providing complete phage resistance (h = 10^{-5}).

Our work has established a broad foundation for using bacterial population dynamics to quantify phage infectivity and bacterial resistance, opening avenues for future work. In particular, empirical work is needed to test the patterns and predictions from this paper. This includes experimental validation of the relationships among metrics (Fig. 2) and between metrics and phage growth rate (Fig. 4), but especially to quantify relationships between phage traits and population dynamic metrics (Figs. 3 and 5 and *SI Appendix*, Figs. S2 and S3). Additional empirical work is also needed to strengthen our understanding of the relationship between cell density and measured proxies of cell density like optical density (84–87), especially over longer timescales where some cells may become resistant or debris may play a role [Fig. 8 and *SI Appendix*, Fig. S27, (9)]. Both empirical and theoretical work are needed to better understand how bacterial susceptibility to phages changes across the phases of bacterial growth (51, 55–59), something our simulations generally ignored (but see Fig. 8). At the same time, future theoretical work should test the capacity and limitations of fitting-based approaches to quantify phage infectivity from bacterial population dynamics. Theory should also explore how additional biological processes alter population dynamics and the inference of infectivity, including lysogeny, stochasticity, failed infections, coinfection exclusion, cooperation, or continuous intrapopulation trait variation. Finally, theory should also be applied to improve our understanding of other methods of quantifying infectivity, like the efficiency of plaquing assay (88).

In all, we have shown that bacterial population dynamics can enable powerful quantification of phage-bacteria interactions. Our findings open the door to a range of applications. For example, growth curves in a microplate reader could be used to rapidly screen libraries of candidate therapeutic phages for efficacy against specific or diverse strains of bacterial pathogens, or to quantify how phages reduce bacterial density, suppress bacterial regrowth, or both. Given that such approaches are already widely used heuristically in the phage-bacteria literature, our findings suggest that they may be ripe for quantitative application from basic to applied questions.

Data, Materials, and Software Availability. There are no data underlying this work.

ACKNOWLEDGMENTS. Thanks to Alita Burmeister, Tiffany Hamidjaja, Catherine Hernandez, Jordan Lewis, Albert Vill, and Caroline Turner for feedback on the manuscript. Thanks to members of the Turner lab for feedback on the work in this project. Thanks to Teresa Carter for contributions to very early work on this project. Thanks to the Yale Institute for Biospheric Studies and HHMI for funding supporting this work. Thanks to the Yale Science, Technology and Research Scholars (STARS) program for funding supporting W.A. during this project.

1. H. G. Hampton, B. N. J. Watson, P. C. Fineran, The arms race between bacteria and their phage foes. *Nature* **577**, 327–336 (2020).
2. J. Antonovics *et al.*, The origin of specificity by means of natural selection: Evolved and nonhost resistance in host-pathogen interactions. *Evolution* **67**, 1–9 (2013).
3. T. Jagdish, A. N. Nguyen Ba, Microbial experimental evolution in a massively multiplexed and high-throughput era. *Curr. Opin. Genet. Dev.* **75**, 101943 (2022).
4. T. Glonti, J.-P. Pirnay, In vitro techniques and measurements of phage characteristics that are important for phage therapy success. *Viruses* **14**, 1490 (2022).
5. E. Kutter, "Phage Host Range and Efficiency of Plating" in Bacteriophages: Methods and Protocols in *Isolation, Characterization, and Interactions, Methods in Molecular Biology*, M. R. J. Clokie, A. M. Kropinski, Eds. (Humana Press, 2009), vol. 1, pp. 141–149.
6. A. M. Kropinski, A. Mazzocco, T. E. Waddell, E. Lingohr, R. P. Johnson, "Enumeration of Bacteriophages by Double Agar Overlay Plaque Assay" in *Bacteriophages: Methods and Protocols, Volume 1: Isolation, Characterization, and Interactions, Methods in Molecular Biology*, M. R. J. Clokie, A. M. Kropinski, Eds. (Humana Press, 2009), pp. 69–76.
7. A. Mazzocco, T. E. Waddell, E. Lingohr, R. P. Johnson, "Enumeration of Bacteriophages by the Direct Plating Plaque Assay" in *Bacteriophages: Methods and Protocols, Volume 1: Isolation, Characterization, and Interactions, Methods in Molecular Biology*, M. R. J. Clokie, A. M. Kropinski, Eds. (Humana Press, 2009), pp. 77–80.
8. A. Mazzocco, T. E. Waddell, E. Lingohr, R. P. Johnson, "Enumeration of bacteriophages using the small drop plaque assay system" in *Bacteriophages: Methods and Protocols, Volume 1: Isolation, Characterization, and Interactions, Methods in Molecular Biology*, M. R. J. Clokie, A. M. Kropinski, Eds. (Humana Press, 2009), pp. 81–85.
9. J. C. Wohlfarth *et al.*, L-form conversion in Gram-positive bacteria enables escape from phage infection. *Nat. Microbiol.* **8**, 387–399 (2023).
10. Z. Yu *et al.*, Modeling multiphage-bacteria kinetics to predict phage therapy potency and longevity. bioRxiv [Preprint] (2022). https://www.biorxiv.org/content/10.1101/2022.11.11.516137v1, [Accessed 26 July 2023].
11. C. N. Vassallo, C. R. Doering, M. L. Littlehale, G. I. C. Teodoro, M. T. Laub, A functional selection reveals previously undetected anti-phage defence systems in the *E. coli* pangenome. *Nat. Microbiol.* **7**, 1568–1579 (2022).
12. L. Tian *et al.*, Self-assembling nanofibrous bacteriophage microgels as sprayable antimicrobials targeting multidrug-resistant bacteria. *Nat. Commun.* **13**, 7158 (2022).
13. J. H. Doss, N. Barekzi, D. T. Gauthier, Improving high-throughput techniques for bacteriophage discovery in multi-well plates. *J. Microbiol. Methods* **200**, 106542 (2022).
14. M. E. K. Haines *et al.*, Analysis of selection methods to develop novel phage therapy cocktails against antimicrobial resistant clinical isolates of bacteria. *Front. Microbiol.* **12**, 613529 (2021).
15. D. Gelman *et al.*, Clinical phage microbiology: A suggested framework and recommendations for the in-vitro matching steps of phage therapy. *Lancet Microbe* **2**, e555–e563 (2021).
16. K. M. Danis-Wlodarczyk *et al.*, Friends or foes? Rapid determination of dissimilar colistin and ciprofloxacin antagonism of *Pseudomonas aeruginosa* phages. *Pharmaceuticals* **14**, 1162 (2021).
17. E. J. Cano *et al.*, Phage therapy for limb-threatening prosthetic knee *Klebsiella pneumoniae* infection: Case report and in vitro characterization of anti-biofilm activity. *Clin. Infect. Dis.* **73**, e144–e151 (2021).
18. M. Benala *et al.*, A revisited two-step microtiter plate assay: Optimization of in vitro multiplicity of infection (MOI) for coliphage and vibriophage. *J. Virol. Methods* **294**, 114177 (2021).
19. D. Rajnovic, J. Mas, Fluorometric detection of phages in liquid media: Application to turbid samples. *Anal. Chim. Acta* **1111**, 23–30 (2020).
20. D. Ping *et al.*, Hitchhiking, collapse, and contingency in phage infections of migrating bacterial populations. *ISME J.* **14**, 2007–2018 (2020).
21. C. Gu. Liu *et al.*, Phage-antibiotic synergy is driven by a unique combination of antibacterial mechanism of action and stoichiometry. *MBio* **11**, e01462–20 (2020).
22. R. Nir-Paz *et al.*, Successful treatment of antibiotic-resistant, poly-microbial bone infection with bacteriophages and antibiotics combination. *Clin. Infect. Dis.* **69**, 2015–2018 (2019).
23. M. Habusha, E. Tzipilevich, O. Fiyaksel, S. Ben-Yehuda, A mutant bacteriophage evolved to infect resistant bacteria gained a broader host range. *Mol. Microbiol.* **111**, 1463–1475 (2019).
24. C. A. Hernandez, B. Koskella, Phage resistance evolution in vitro is not reflective of in vivo outcome in a plant-bacteria-phage system. *Evolution* **73**, 2461–2475 (2019).
25. S. Aslam *et al.*, Early clinical experience of bacteriophage therapy in 3 lung transplant recipients. *Am. J. Transplant.* **19**, 2631–2639 (2019).
26. F. Forti *et al.*, Design of a broad-range bacteriophage cocktail that reduces *Pseudomonas aeruginosa* biofilms and treats acute infections in two animal models. *Antimicrob. Agents Chemother.* **62**, e02573–17 (2018).
27. R. T. Schooley *et al.*, Development and use of personalized bacteriophage-based therapeutic cocktails to treat a patient with a disseminated resistant *Acinetobacter baumannii* infection. *Antimicrob. Agents Chemother.* **61**, e00954–17 (2017).
28. D. Cho, I. Lau, M. Li, D. Zhu, Development of a microtiter plate assay for real time analysis of T7 bacteriophage mediated lysis of *Escherichia coli*. *J. Exp. Microbiol. Immunol.* **21**, 6 (2017).
29. L. A. Estrella *et al.*, Characterization of novel *Staphylococcus aureus* lytic phage and defining their combinatorial virulence using the OmniLog® system. *Bacteriophage* **6**, e1219440 (2016).
30. J. Bertozzi Silva, D. Sauvageau, Bacteriophages as antimicrobial agents against bacterial contaminants in yeast fermentation processes. *Biotechnol. Biofuels* **7**, 123 (2014).
31. M. Henry, R. Lavigne, L. Debarbieux, Predicting in vivo efficacy of therapeutic bacteriophages used to treat pulmonary infections. *Antimicrob. Agents Chemother.* **57**, 5961–5968 (2013).
32. I.-N. Wang, Lysis timing and bacteriophage fitness. *Genetics* **172**, 17–26 (2006).
33. R. R. Raya *et al.*, Isolation and characterization of a new T-even bacteriophage, CEV1, and determination of its potential to reduce *Escherichia coli* O157:H7 levels in sheep. *Appl. Environ. Microbiol.* **72**, 6405–6410 (2006).
34. S. T. Abedon, P. Hyman, C. Thomas, Experimental examination of bacteriophage latent-period evolution as a response to bacterial availability. *Appl. Environ. Microbiol.* **69**, 7499–7506 (2003).
35. J. B. Lynch, B. D. Bennett, B. D. Merrill, E. G. Ruby, A. J. Hryckowian, Independent host- and bacterium-based determinants protect a model symbiosis from phage predation. *Cell Rep.* **38**, 110376 (2022).
36. M. Henry *et al.*, Development of a high throughput assay for indirectly measuring phage growth using the omnilog TM system. *Bacteriophage* **2**, 159–167 (2012).
37. J. M. Borin, S. Avrani, J. E. Barrick, K. L. Petrie, J. R. Meyer, Coevolutionary phage training leads to greater bacterial suppression and delays the evolution of phage resistance. *Proc. Natl. Acad. Sci. U.S.A.* **118**, e2104592118 (2021).
38. R. M. Ceballos, C. L. Stacy, Quantifying relative virulence: When μ max fails and AUC alone just is not enough. *J. Gen. Virol.* **102**, jgv001515 (2020).
39. C. J. Cooper, S. P. Denyer, J. Y. Maillard, Rapid and quantitative automated measurement of bacteriophage activity against cystic fibrosis isolates of *Pseudomonas aeruginosa*. *J. Appl. Microbiol.* **110**, 631–640 (2011).
40. M. Konopacki, B. Grygorcewicz, B. Dołęgowska, M. Kordas, R. Rakoczy, PhageScore: A simple method for comparative evaluation of bacteriophages lytic activity. *Biochem. Eng. J.* **161**, 107652 (2020).
41. J.-Y. Maillard, T. s. Beggs, M. j. Day, R. a. Hudson, A. d. Russell, The use of an automated assay to assess phage survival after a biocidal treatment. *J. Appl. Bacteriol.* **80**, 605–610 (1996).
42. C. E. Martinez-Soto *et al.*, PHIDA: A high throughput turbidimetric data analytic tool to compare host range profiles of bacteriophages isolated using different enrichment methods. *Viruses* **13**, 2120 (2021).
43. D. Rajnovic, X. Muñoz-Berbel, J. Mas, Fast phage detection and quantification: An optical density-based approach. *PLoS ONE* **14**, e0216292 (2019).
44. Z. J. Storms, M. R. Teel, K. Mercurio, D. Sauvageau, The virulence index: A metric for quantitative analysis of phage virulence. *PHAGE* **1**, 27–36 (2020).

45. P. E. Turner, J. A. Draghi, R. Wilpiszeski, High-throughput analysis of growth differences among phage strains. *J. Microbiol. Methods* **88**, 117–121 (2012).
46. Y. Xie, L. Wahab, J. Gill, Development and validation of a microtiter plate-based assay for determination of bacteriophage host range and virulence. *Viruses* **10**, 189 (2018).
47. Y. Geng, T. V. P. Nguyen, E. Homaee, I. Golding, Using bacterial population dynamics to count phages and their lysogens. *Nat. Commun.* **15**, 7814 (2024).
48. P. E. Sørensen *et al.*, Classification of in vitro phage-host population growth dynamics. *Microorganisms* **9**, 2470 (2021).
49. Y. Mulla, J. Müller, D. Trimcev, T. Bollenbach, Extreme diversity of phage amplification rates and phage–antibiotic interactions revealed by PHORCE. bioRxiv [Preprint] (2024), https://www.biorxiv.org/content/10.1101/2024.06.07.597930v3, [Accessed 27 February 2025].
50. N. Hosseini, M. Chehreghani, S. Moineau, S. J. Charette, Centroid of the bacterial growth curves: A metric to assess phage efficiency. *Commun. Biol.* **7**, 1–9 (2024).
51. C. Igler, Phenotypic flux: The role of physiology in explaining the conundrum of bacterial persistence amid phage attack. *Virus Evol.* **8**, veac086 (2022).
52. J. S. Weitz, *Quantitative Viral Ecology: Dynamics of Viruses and Their Microbial Hosts* (Princeton University Press, 2015).
53. J. J. Bull, S. M. Krone, Mathematical comparison of protocols for adapting a bacteriophage to a new host. *Virus Evol.* **10**, veae100 (2024).
54. B. R. Levin, F. M. Stewart, L. Chao, Resource-limited growth, competition, and predation: A model and experimental studies with bacteria and bacteriophage. *Am. Nat.* **111**, 3–24 (1977).
55. B. Koskella, C. A. Hernandez, R. M. Wheatley, Understanding the impacts of bacteriophage viruses: From laboratory evolution to natural ecosystems. *Annu. Rev. Virol.* **9**, 57–78 (2022).
56. M. Choua, J. A. Bonachela, Ecological and evolutionary consequences of viral plasticity. *Am. Nat.* **193**, 346–358 (2019).
57. D. Nabergoj, P. Modic, A. Podgornik, Effect of bacterial growth rate on bacteriophage population growth rate. *Microbiolopen* **7**, e00558 (2018).
58. D. Bryan, A. El-Shibiny, Z. Hobbs, J. Porter, E. M. Kutter, Bacteriophage T4 infection of stationary phase *E. coli*: Life after log from a phage perspective. *Front. Microbiol.* **7**, 1391 (2016).
59. H. Hadas, M. Einav, I. Fishov, A. Zaritsky, Bacteriophage T4 development depends on the physiology of its host *Escherichia coli*. *Microbiology* **143**, 179–185 (1997).
60. S. J. Schrag, J. E. Mittler, Host-parasite coexistence: The role of spatial refuges in stabilizing bacteria-phage interactions. *Am. Nat.* **148**, 348–377 (1996).
61. J. J. Bull, C. S. Vegge, M. Schmerer, W. N. Chaudhry, B. R. Levin, Phenotypic resistance and the dynamics of bacterial escape from phage control. *PLoS ONE* **9**, e94690 (2014).
62. K. Soetaert, T. Petzoldt, R. W. Setzer, Solving differential equations in R: Package deSolve. *J. Stat. Softw.* **33**, 1–25 (2010).
63. M. Blazanin, gcplyr: An R package for microbial growth curve data analysis. *BMC Bioinformatics* **25**, 232 (2024).
64. M. A. Brockhurst, A. D. Morgan, A. Fenton, A. Buckling, Experimental coevolution with bacteria and phage. The Pseudomonas fluorescens–Φ2 model system. *Infect. Genet. Evol.* **7**, 547–552 (2007).
65. M. Blazanin, J. Moore, S. Olsen, M. Travisano, Fight not flight: Parasites drive the bacterial evolution of resistance. Not escape. *Am. Nat.* **205**, 125–136 (2025).
66. Y. Shao, I.-N. Wang, Bacteriophage adsorption rate and optimal lysis time. *Genetics* **180**, 471–482 (2008).
67. R. H. Heineman, J. J. Bull, Testing optimality with experimental evolution: Lysis time in a bacteriophage. *Evolution* **61**, 1695–1709 (2007).
68. R. W. Reader, L. Siminovitch, Lysis defective mutants of bacteriophage lambda: Genetics and physiology of S cistron mutants. *Virology* **43**, 607–622 (1971).
69. R. Gallet, Y. Shao, I.-N. Wang, High adsorption rate is detrimental to bacteriophage fitness in a biofilm-like environment. *BMC Evol. Biol.* **9**, 241 (2009).
70. R. Josslin, The lysis mechanism of phage T4: Mutants affecting lysis. *Virology* **40**, 719–726 (1970).
71. H. M. Lindberg, K. A. McKean, I.-N. Wang, Phage fitness may help predict phage therapy efficacy. *Bacteriophage* **4**, e964081 (2014).
72. M. D. Paepe, F. Taddei, Viruses' life history: Towards a mechanistic basis of a trade-off between survival and reproduction among phages. *PLoS Biol.* **4**, e193 (2006).
73. Y. Shao, I.-N. Wang, Effect of late promoter activity on bacteriophage λ fitness. *Genetics* **181**, 1467–1475 (2009).
74. N. Dufour, R. Delattre, J.-D. Ricard, L. Debarbieux, The lysis of pathogenic *Escherichia coli* by bacteriophages releases less endotoxin than by β-lactams. *Clin. Infect. Dis.* **64**, 1582–1588 (2017).
75. R. C. T. Wright, V.-P. Friman, M. C. M. Smith, M. A. Brockhurst, Cross-resistance is modular in bacteria–phage interactions. *PLoS Biol.* **16**, e2006057 (2018).
76. A. R. Burmeister *et al.*, Pleiotropy complicates a trade-off between phage resistance and antibiotic resistance. *Proc. Natl. Acad. Sci. U.S.A.* **117**, 11207–11216 (2020).
77. B. A. Duerkop, W. Huo, P. Bhardwaj, K. L. Palmer, L. V. Hooper, Molecular basis for lytic bacteriophage resistance in enterococci. *mBio* **7**, e01304 (2016). 10.1128/mbio.01304-16.
78. M. Demerec, U. Fano, Bacteriophage-resistant mutants in *Escherichia coli*. *Genetics* **30**, 119–136 (1945).
79. W. R. King, E. B. Collins, E. L. Barrett, Frequencies of bacteriophage-resistant and slow acid-producing variants of *Streptococcus cremoris*. *Appl. Environ. Microbiol.* **45**, 1481–1485 (1983).
80. H. Schenk, M. Sieber, Bacteriophage can promote the emergence of physiologically sub-optimal host phenotypes. bioRxiv [Preprint] (2019), https://www.biorxiv.org/content/10.1101/621524v1, [Accessed 19 April 2023].
81. A. L. Lloyd, Destabilization of epidemic models with the inclusion of realistic distributions of infectious periods. *Series B: Biol. Sci.* **267**, 985–993 (2001).
82. T. Sauer *et al.*, Identifiability of infection model parameters early in an epidemic. *SIAM J. Control Optim.* **60**, S27–S48 (2022).
83. O. Melikechi *et al.*, Limits of epidemic prediction using SIR models. *J. Math. Biol.* **85**, 36 (2022).
84. J. A. Myers, B. S. Curtis, W. R. Curtis, Improving accuracy of cell and chromophore concentration measurements using optical density. *BMC Biophys.* **6**, 4 (2013).
85. J. Beal *et al.*, Robust estimation of bacterial cell count from optical density. *Commun. Biol.* **3**, 1–29 (2020).
86. K. Stevenson, A. F. McVey, I. B. N. Clark, P. S. Swain, T. Pilizota, General calibration of microbial growth in microplate readers. *Sci. Rep.* **6**, 38828 (2016).
87. P. Mira, P. Yeh, B. G. Hall, Estimating microbial population data from optical density. *PLoS ONE* **17**, e0276040 (2022).
88. R. Gallet, S. Kannoly, I. N. Wang, Effects of bacteriophage traits on plaque formation. *BMC Microbiol.* **11**, 181 (2011).